Journal of Applied Polymer Science

Synergistic effect of graphite nanoplatelets and glass fibers in polypropylene composites

Diego Pedrazzoli,[1,2] Alessandro Pegoretti,[1] Kyriaki Kalaitzidou[2,3]

[1]Department of Industrial Engineering and INSTM Research Unit, University of Trento, Trento 38123, Italy
[2]G. W. Woodruff School of Mechanical Engineering, Georgia Institute of Technology, Atlanta, Georgia 30336
[3]School of Materials Science and Engineering, Georgia Institute of Technology, Atlanta, Georgia 30322
Correspondence to: D. Pedrazzoli (E-mail: pedrazzoli.diego@gmail.com)

ABSTRACT: In this study, polypropylene (PP) composites reinforced with short glass fibers (GF) and exfoliated graphite nanoplatelets were obtained by melt compounding followed by injection molding. Morphological observations and quasi-static tensile tests were carried out in order to investigate how the morphology and the mechanical properties of the composites were affected by the combined effect of two fillers of rather different size scales (i.e., micro- and nanoscale). The results indicate that the dispersion of the nanofiller in the PP matrix promoted the formation of a stronger interface between the matrix and GF, as indicated by the increase of the interfacial shear strength determined by the single-fiber microdebonding test. Concurrently, a significant improvement of the tensile modulus and impact strength of the composites was observed, with small changes in the processability of hybrid composites compared to that of GF composites, as confirmed by rheological measurements. © 2014 Wiley Periodicals, Inc. J. Appl. Polym. Sci. **2015**, *132*, 41682.

KEYWORDS: composites; graphene and fullerenes; mechanical properties; nanotubes; structure-property relations; viscosity and viscoelasticity

Received 25 July 2014; accepted 29 October 2014
DOI: 10.1002/app.41682

INTRODUCTION

Fiber-reinforced polymer composites are widely used in structural applications in the aerospace, automotive, civil, and marine arenas, especially due to their high specific stiffness and strength, chemical and weather resistances, tailorable mechanical, thermal and electrical properties.[1] In case of glass fiber (GF) reinforced thermoplastics, GF loadings of 30–50 wt % are quite common[2] and required to achieve the desired performances. However, high fiber loadings usually lead to an undesirable increase in density, decreased melt flow, and increased brittleness.[3] For short fibers, their reinforcement efficiency is governed largely by the fiber concentration and aspect ratio, fiber adhesion to the matrix, fiber orientation, and its dispersion within the matrix.[4]

Among thermoplastic matrices, polypropylene (PP) is one of the most widely used for GF-reinforced composites.[5] Short-fiber reinforced composites are much less resistant to mechanical load and fatigue damage than the corresponding continuous-fiber-reinforced materials, mainly because the weak matrix has to sustain a greater proportion of the load.[6] On the other hand, polymer nanocomposites reinforced with nanofillers such as silica, exfoliated graphite, and carbon nanotubes have recently attracted great interest due to the considerable enhancement in stiffness realized at low filler loadings i.e. < 7 wt %[7,8] and substantial improvements in mechanical,[9] thermal,[10] and flammability[11] properties with no significant increase of the density.[12] However, addition of more than 10 wt % of nanofiller leads to poor dispersion and processing characteristics.[13] Furthermore, as recently reported, nanoparticles can play a beneficial role on the interfacial properties of structural composites,[14,15] and can induce functional properties such as thermal and electrical conductivity.[16,17]

The aim of this study is to investigate how the morphology, rheology, and specific mechanical properties of GF-reinforced PP composites are affected by the presence of exfoliated graphite nanoplatelets (GNP). Moreover, the investigation of the stress-transfer mechanism at the fiber/matrix interface is another primary objective of this research. The ultimate goal is to explore whether the combination of two fillers of rather different size scales can create synergistic effects and lead to hybrid composites that perform better than the single filler composites (i.e., GF/ composites), are lighter, and easier to process. Presently, only few preliminary studies have been reported on the structure and properties of GF-reinforced polymer nanocomposites.[4,18,19] In

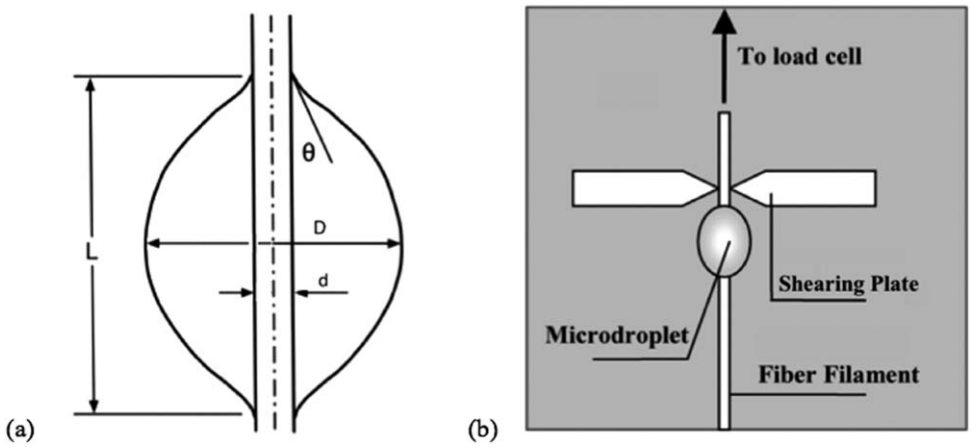

Figure 1. (a) Schematic representation of a matrix drop deposited onto a rigid fiber and (b) schematic of the microdebonding test (right).

particular, Jacob *et al.* investigated PP reinforced with nylon microfiber and nanosilica, pointing out a significant synergistic effect on the mechanical properties of the composite, including tensile strength and modulus, flexural strength and modulus, and impact strength in some cases.[4] In a similar way, Vlasveld *et al.* showed that a polyamide-6 matrix reinforced with platelets of exfoliated layered silicate and short GF displays improved stiffness and yielding behavior.[19] However, the current literature still lacks contributes regarding deeper investigations on possible synergistic effects on the mechanical behavior of the composites as promoted by enhanced fiber/matrix interfacial properties.

EXPERIMENTAL

Materials and Processing of Composites

An isotactic homopolymer PP with the trade name PPH-B-10-FB (MFI at 190°C and 2.16 kg = 6.9 g/10′, density = 0.904 g/cm^3) produced by Polychim Industrie s.a.s. (Loon-Plage, France) was used. Fusabond® P M-613-05 maleic anhydride modified PP, PP-*g*-MA, (MFI = 106.8 g/10′at 190°C and 2.16 kg, 0.903 g/cm^3, maleic anhydride content = 0.35–0.70 wt %), by DuPont™ was used as compatibilizer. Exfoliated GNP xGnP®-M5 from XG Sciences, with an average diameter of ~5 μm and thickness in the range of 10–20 nm were used. Finally, E-glass fibers, RO99 P319, by Saint-GobainVetrotex, were used as-received. The GF are surface treated with a silane-based coupling agent specifically designed for PP. Chopped strand GF (single fiber diameter of 15.3 ± 1.5 μm, and average length of 6.50 ± 0.44 mm) were obtained by chopping long GF using a chopper gun. Graphite coated GF were prepared by sonication of GNP in isopropanol at a concentration of 5 mg/mL using a sonicator Misonix S-4000-010 for 1 h (30% amplitude, 8 W power) equipped with a probe of 12.5 mm diameter. After adding the GF to the solution, sonication was continued for 0.5 h. The GNP coated GF were rinsed in isopropanol and dried in a hood overnight.

Composites were made by melt mixing and injection molding using a vertical, co-rotating, bench-top twin-screw micro-extruder (DSM Micro 15 cm^3 Compounder) connected to a micro-injection molding unit (DSM), in order to obtain dumb-bell specimens according to the standard ASTM D638. The compound was mixed for 3 min, at 190°C and 250 rpm. After the polymer compound had melted and homogenized, short GF strands were directly added to the melt and further mixed for 2 min before injection molding. The mold temperature was 80°C and the injection pressure was 800 kPa.

The PP-*g*-MA was added at 1 : 1 ratio with respect to the GNP. The composites are designated as follows: the kind of filler with its content, the compatibilizer (if any) with its content, and the matrix. For instance, the composite filled with 5 wt % of PP-g-MA, 5 wt % of xGnP-M5, and 10 wt % GF was indicated as 5GNP/10GF/5PP-*g*-MA/PP. Coated GF are indicated as GFc.

Characterization of Composites

Thin (70–80 μm) films required for the analysis of the GF length distribution were obtained by compression molding (at 200°C and 4 MPa, for 10 min) of the dogbone specimens produced by injection molding, and were observed with an optical microscope Leica DMRM (Leica Microsystems) through a video-camera DFC 420. The reported average fiber length is an average of at least 200 measurements. The fracture surfaces of the composites were studied using a Phenom G2 Pro (Phenom-World BV) scanning electron microscope (SEM), at an acceleration voltage of 5 kV. For in-plane observations, the dogbone specimens were chemically etched (60 g CrO_3/100 mL H_2O, at 70°C for 24 h). Prior to the SEM study, a thin gold coating was applied onto the surface to minimize charging effects.

The effect of the GNP on the fiber–matrix adhesion was investigated through microdebonding tests performed on specimens consisting of a PP microdrop solidified onto a single fiber filament supported on a paper tab. In order to avoid formation of asymmetric droplets with respect to the filament, a PP fiber was tied around the filament prior to heating[20] that was done using a hot stage (Instec HCS302) placed under an optical microscope. Prior to testing, the microbond samples were examined using an optical microscope in order to determine the fiber diameter (d), embedded fiber length (L), and the maximum droplet diameter (D) shown schematically in Figure 1(a). Microdebonding tests were conducted at a crosshead speed of

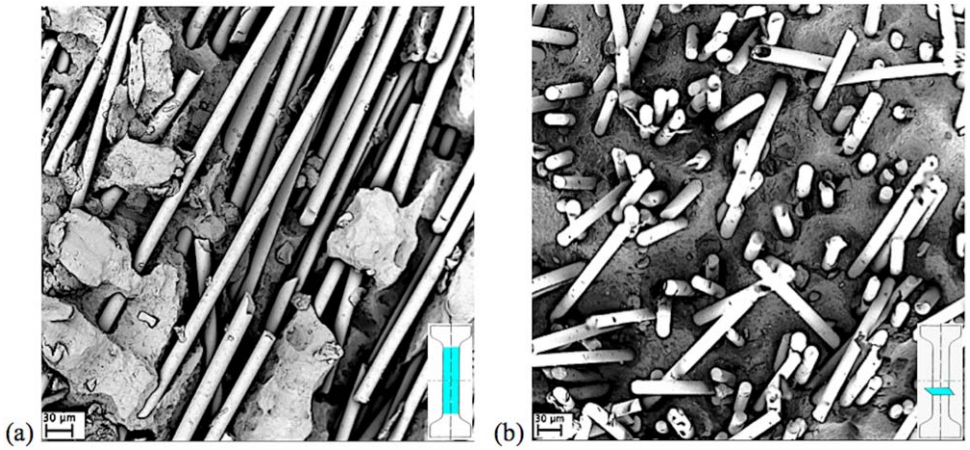

Figure 2. SEM observations of chemically etched surfaces of 30GF/PP composite considering (a) the in-plane section and (b) the cross-section of a dog-bone specimen. [Color figure can be viewed in the online issue, which is available at wileyonlinelibrary.com.]

1 mm/min by an Instron 33R 4466 tensile tester equipped with a 500 N load cell. During testing the paper tab attached to one end of the GF was slowly pulled up, while the droplet was constrained by a shearing plate, fixed on a stationary support as shown in Figure 1(b). The interfacial shear strength (ISS), τ, was computed by eq. (1):

$$\tau = \frac{F_c}{\pi d L} \tag{1}$$

where F_c is the critical applied load, recorded during the test, at which the fiber–matrix interface fails. The single fiber specimens were observed by SEM before and after the test.

Melt rheology of the composites was analyzed by an ARES-G2 rheometer by TA Instruments, under controlled strain conditions and using a parallel plate geometry with 25 mm plate diameter. Isothermal frequency sweep tests in the range 0.1–200 rad/s were carried out at 180°C using a small amplitude (10%) oscillatory shear. Noteworthy, a preliminary analysis was carried out to verify the linear viscoelastic response of the material under the testing condition. Each data point reported is an average of at least three measurements.

Tensile tests at a crosshead speed of 5 mm/min were performed at room temperature according to ASTM D638 with an Instron model 33R 4466 tensile tester equipped with a 500 N load cell. Axial strain was recorded using a 10 mm gauge length extensometer Instron® model 2630-101. The elastic modulus was measured as secant modulus between longitudinal deformation levels of 0.05% and 0.25%. Dynamic mechanical analyses (DMA) were carried out in tensile mode by a DMA Q800 by TA Instruments, from 20°C to 160°C, at 5°C/min and 1 Hz. A preload of 0.2 MPa and a maximum strain of 0.05% were imposed on rectangular samples 25 mm long, 3.30 mm wide, and 3.27 mm thick. Izod impact tests were performed according to the ASTM D256 standard using a pendulum by Custum Scientific Instruments.

Micromechanical Models for Hybrid Composites

Micromechanics-based models, such as Halpin–Tsai (H-T) and Mori–Tanaka, are commonly used to predict the tensile modulus of composites containing a single filler.[21,22] Recently, two-population models have been proposed to study the combined effect of exfoliated montmorillonite and intercalated tactoids[23] and the effects of organoclay and GF in Nylon 6 hybrid composites.[24] Such models can be described by the following equation based on the additive approach:

$$\frac{E_{\text{hybrid}}}{E_m} = \frac{E_{\text{GF}}}{E_m} + \frac{E_{\text{nc}}}{E_m} - 1 \tag{2}$$

where E_{hybrid} is the modulus of the hybrid composite, E_{GF} and E_{nc} is the modulus of the GF-reinforced composite and the nanocomposite, respectively, while E_{m} is the modulus of the neat matrix. In the additive approach, the contributions of each filler are calculated separately and added together without double counting the matrix contribution. The H-T model was employed to predict the tensile modulus of the nanocomposites.[22] The parameter ξ of the H-T model is assumed as $2/3a$, where a is the GNP aspect ratio. The GNP elastic modulus is assumed as 70 GPa.[25] This model accounts for the modulus of the consituents and fillers' geometry and aspect ratio, and assumes perfect contact at the polymer/filler interface, homogeneous dispersion and distribution and unidirectional filler orientation along the applied load direction.[26] Due to this last assumption, the model is not ideal for the prediction of E_{GF}. In fact, the GF appear highly oriented in the longitudinal direction due to the injection molding, as shown in the in-plane images of the 30GF/PP composite [Figure 2(a)], but a significant misalignment can be observed in the out-of-plane direction [Figure 2(b)]. Thus, in addition to the H-T model, the Tsai and Pagano (T-P) model,[27] that accounts for randomly in-plane oriented short-fibers, was also applied to predict E_{GF}, considering the elastic modulus of the fibers as 63 GPa.[28]

The aspect ratio of the fibers, an input parameter in both models, was determined experimentally by measuring the fiber length distribution in composite films by optical image analysis. The weight ($\overline{L_w}$) average fiber length was calculated by eq. (3):

$$\overline{L_w} = \frac{\sum n_i L_i^2}{\sum n_i L_i} \tag{3}$$

where n_i is the occurring frequency of GF with length in the rangle of L_i. $\overline{L_w}$ is divided by the mean fiber diameter to

Table I. Mechanical and Morphological Properties of the Composites

Sample	E (GPa), E* [GPa/(g/cm^3)]	σ_B (MPa), σ_B^* [MPa/(g/cm^3)]	ε_B (%)	Izod impact strength (J/m)	Weight av. GF aspect ratio
PP	2.06 ± 0.08, 2.23	38.5 ± 0.7[a], 42.6	8.9 ± 0.5[b]	15.8 ± 1.4	/
30GF/PP	4.69 ± 0.08, 4.20	43.1 ± 0.7, 38.6	2.8 ± 0.2	46.2 ± 2.0	19.8
10GF/PP	3.21 ± 0.08, 3.32	41.8 ± 0.3, 43.3	6.3 ± 0.5	34.2 ± 1.8	23.1
10GFc/PP	3.56 ± 0.03, 3.69	41.8 ± 0.3, 43.3	5.9 ± 0.1	36.3 ± 1.4	22.1
1GNP/10GF/PP	3.57 ± 0.07, 3.67	43.8 ± 0.4, 45.1	4.7 ± 0.2	/	21.3
3GNP/10GF/PP	3.66 ± 0.13, 3.74	43.8 ± 0.4, 44.4	4.4 ± 0.2	/	20.9
5GNP/10GF/PP	4.26 ± 0.14, 4.30	43.9 ± 0.1, 44.4	3.6 ± 0.1	42.2 ± 2.4	20.0
5GNP/10GFc/PP	4.47 ± 0.08, 4.52	45.4 ± 0.8, 45.9	4.1 ± 0.2	45.0 ± 1.9	19.2
7GNP/10GF/PP	4.43 ± 0.06, 4.43	43.7 ± 0.3, 43.7	3.6 ± 0.1	/	18.7
5GNP/15GF/PP	4.67 ± 0.05, 4.56	44.8 ± 0.5, 43.7	3.6 ± 0.2	46.0 ± 1.6	16.7
5GNP/10GF/ 5PP-*g*-MA/PP	4.29 ± 0.09, 4.33	49.1 ± 0.3, 49.6	4.1 ± 0.2	50.0 ± 1.6	20.8

[a,b]Ultimate tensile strength and corresponding strain, respectively.
E, *E**: Elastic modulus and corresponding specific value.
σ_B, σ_B^*: Tensile strength and corresponding specific value.
ε_B: Strain at break.

compute the weight average aspect ratio of the GFs (i.e., $\overline{R_w} = \overline{L_w} / \overline{d}$). For all composites, there is a substantial decrease in fiber length with GF content (Table I), attributed to the increase in viscosity which leads to higher frictional stresses generated during melt processing. Concurrently, when GNP is added to systems loaded with 10 wt % GF, the viscosity of the nanocomposite matrix further increases and higher shear stresses are expected in the presence of the fibers. Moreover, as already reported, the nanoparticle impingement on the fiber surfaces occurring during melt processing in GF/Nylon 6 modified with organoclay[24] can be another reason for increased GF attrition especially at high filler concentrations.

RESULTS AND DISCUSSION

Interfacial Shear Strength

The micrograph of a microdebonding single fiber specimen, reported in Figure 3(a), indicates that the PP microdrop with a diameter of around 870 μm appears to be quite symmetrically centered with respect to the fiber axis. The interfacial failure mechanism during debonding was assessed by SEM investigation of the microdrop interface before [Figure 3(b)] and after [Figure 3(c)] the microdebonding test. As shown, the fracture zone shows evident interfacial debonding and limited matrix cracking. As it clearly emerges from Figure 4, the incorporation of GNP results in a noticeable increase of the failure shear stress evaluated at the interface (ISS), indicating a substantial enhancement of the load transfer between fiber and matrix. It is worthwhile to note that the ISS values are in good agreement with those estimated through the single-fiber fragmentation test (SFFT) on model GF/PP composites systems modified with the addition of GNP.[15] Similar effects have also been observed when both non-functionalized and dimethyldichlorosilane-functionalized silica nanoparticles are dispersed in the PP matrix and a remarkable increase in interfacial strength is detected in GF/PP systems.[28] However, the greatest improvement is reached in the compatibilized system (i.e., 5GNP/GF/5PP-*g*-MA/PP), with a clear synergistic effect of PP-*g*-MA and nanofiller. In particular, PP-*g*-MA is supposed not only to improve the nanofiller dispersion, but also to significantly enhance the chemical affinity between PP and GNP and between PP and GF.[28] Interestingly, a slightly improved ISS can be observed also when coated GF were used (i.e., GFc/PP and 5GNP/GFc/PP), with a positive effect of the GNP fiber coating on the ISS.

Morphology Characterization

SEM micrographs of fracture surfaces for PP composites loaded with 10 wt % GF are shown in Figure 5(a). The GFs are generally homogeneously dispersed in the PP matrix, and several fibers are pulled out from the matrix. Interfacial debonding appears to be the dominant failure mechanism, indicating a rather low adhesion level. On the other hand, a different failure behavior is observed for hybrid PP composites containing 5 wt % GNP and 10 wt % GF [Figure 5(b)] and 5 wt % PP-*g*-MA, 5 wt % GNP and 10 wt % GF [Figure 5(c)]. In this case, very few debonded fibers can be observed indicating a significantly better fiber–matrix adhesion. Furthermore, the improved fiber/matrix compatibility is documented by the presence of matrix residuals on the fiber surface after pull-out. The effectiveness of GFs coating, when considering the 5GNP/10GFc/PP composite, is evidenced by the presence of some graphite residuals on the fiber surface after the pull-out [Figure 5(d)].

Tensile Properties of Hybrid Composites

The tensile modulus (E), tensile strength (σ_B), and strain at break (ε_B) of the hybrid composites, as a function of the GNP content, are presented in Table I along with the specific modulus (E^*) and the specific tensile strength (σ_B^*). It can be observed that at constant GF content of 10 wt %, the moduli E and E^* significantly increase with GNP content, the σ_B and σ_B^* values initially increase reaching a plateau and ε_B decreases with GNP content. The increase of σ_B at low and intermediate GNP

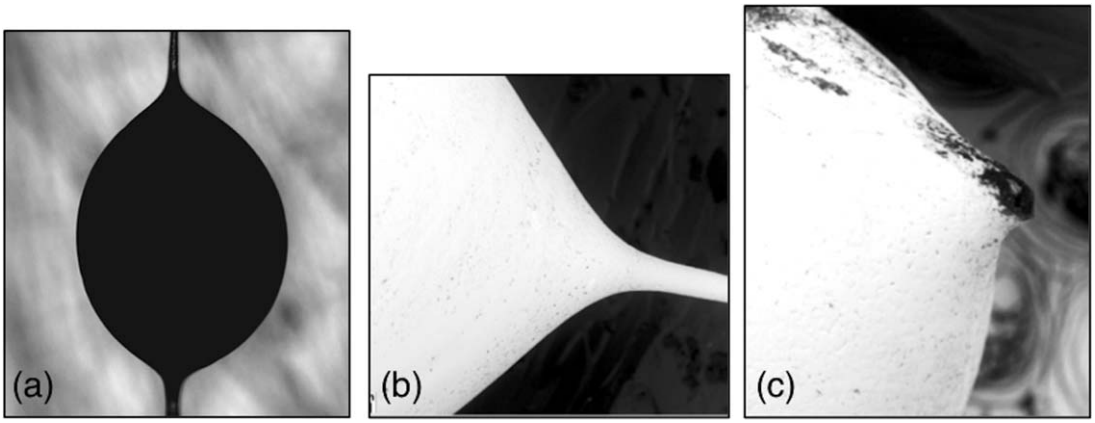

Figure 3. SEM images of (a) neat PP drop deposited on a GF for the microdebonding tests, (b) magnification at the fiber/drop interface before microdebonding, and (c) detail of the interface after debonding.

contents is certainly promoted by the enhancement of the GF/PP interfacial shear strength and the consequent more efficient stress transfer. The hybrid composites are thus lighter and stronger than the GF composites. When GNP-coated GF are used (i.e., 10GFc/PP and 5GNP/10GFc/PP composites), which means that the GNP is introduced at the GF/PP interface, the composites exhibit slightly higher $E^{\star}$ and σ_B^* compared to the corresponding composites 10GF/PP and 5GNP/10GF/PP, where the GNP is only added directly in the bulk PP matrix by melt compounding. Again, this peculiar behavior could be attributed to stronger GF–PP interfacial interactions. Addition of PP-*g*-MA compatibilizer results in a significant increase of σ_B, also evidencing stronger interactions at the interface.

Theoretical Prediction of Modulus versus Experimental Results in Hybrid Composites

The tensile modulus predictions for hybrid composites, E_{hybrid}, as a function of GNP content, applying the additive two-population method [eq. (2)], are presented in Figure 6. E_{nc} is calculated using the H-T model and considering two different GNP's aspect ratios *a*: (i) $a = 250$ based on info provided by the supplier and (ii) $a = 80$ as estimated from SEM observations accounting filler agglomeration. E_{GF} is calculated using either the H-T or the T-P models. When the H-T model is used for E_{GF}, the theoretical E_{hybrid} is significantly higher than the experimental values obviously because the model assumes unidirectional alignment of both the GNP and GF. Independently from the model used to calculate E_{GF}, the higher the aspect ratio of the GNP, the higher the E_{hybrid}, as expected. Furthermore, as shown in the figure, the effect of the aspect ratio (extent of agglomeration) becomes significant only at higher GNP contents. Therefore, using the H-T for E_{GF} and the T-P for E_{GF} one can get the upper and lower limits of E_{hybrid}. The results are in agreement with the morphological observations, as the hybrid composites exhibit only partial in-plane alignment of the fibers.

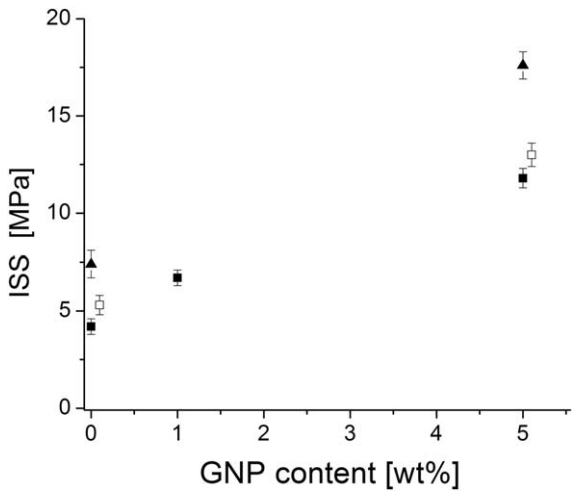

Figure 4. Interfacial shear strength values of GF/PP composites as a function of the GNP amount, considering uncoated (full point) and coated (open point) GFs, while (▲) indicates the system GF/5PP-*g*-MA/PP and 5GNP/GF/5PP-*g*-MA/PP.

Impact Strength

Significant differences in the impact resistance of the composites can be observed with the addition of only 5 wt % GNP (Table I). The impact resistance has increased by more than 10%. The increase in resistance under impact conditions exhibited by the hybrid composites at low filler loadings can be ascribed to (i) changes in the energy absorbing mechanisms (i.e., higher plastic deformation of the matrix along the filler/matrix interface, crack branching due to hindrance by reinforcements, bridging of the crack, creation of voids etc.) and (ii) different crystalline morphology (i.e., spherulite size and polymorphism) occurring upon nanomodification.[29,30] However, the toughening effect provided by high modulus filler particles ($E \sim 70$ GPa for GNP) is limited by nanofiller agglomeration.

As expected, the impact resistance increases with the GF loading, while significant improvements can be observed when coated GF are used compared to the systems based on uncoated GF. The enhancement in impact resistance corresponds to 6.1% and 6.6% when 10GFc/PP and 5GNP/10GFc/PP, are considered respectively. Remarkable impact resistance is also exhibited by the composite 5GNP/10GF/5PP-*g*-MA/PP containing compatibilizer.

Viscoelastic Behavior in the Melt State and in the Solid State

The effect of the GF addition on the dynamic shear storage modulus (G') and complex viscosity ($|\eta^{\star}|$) at melt temperature

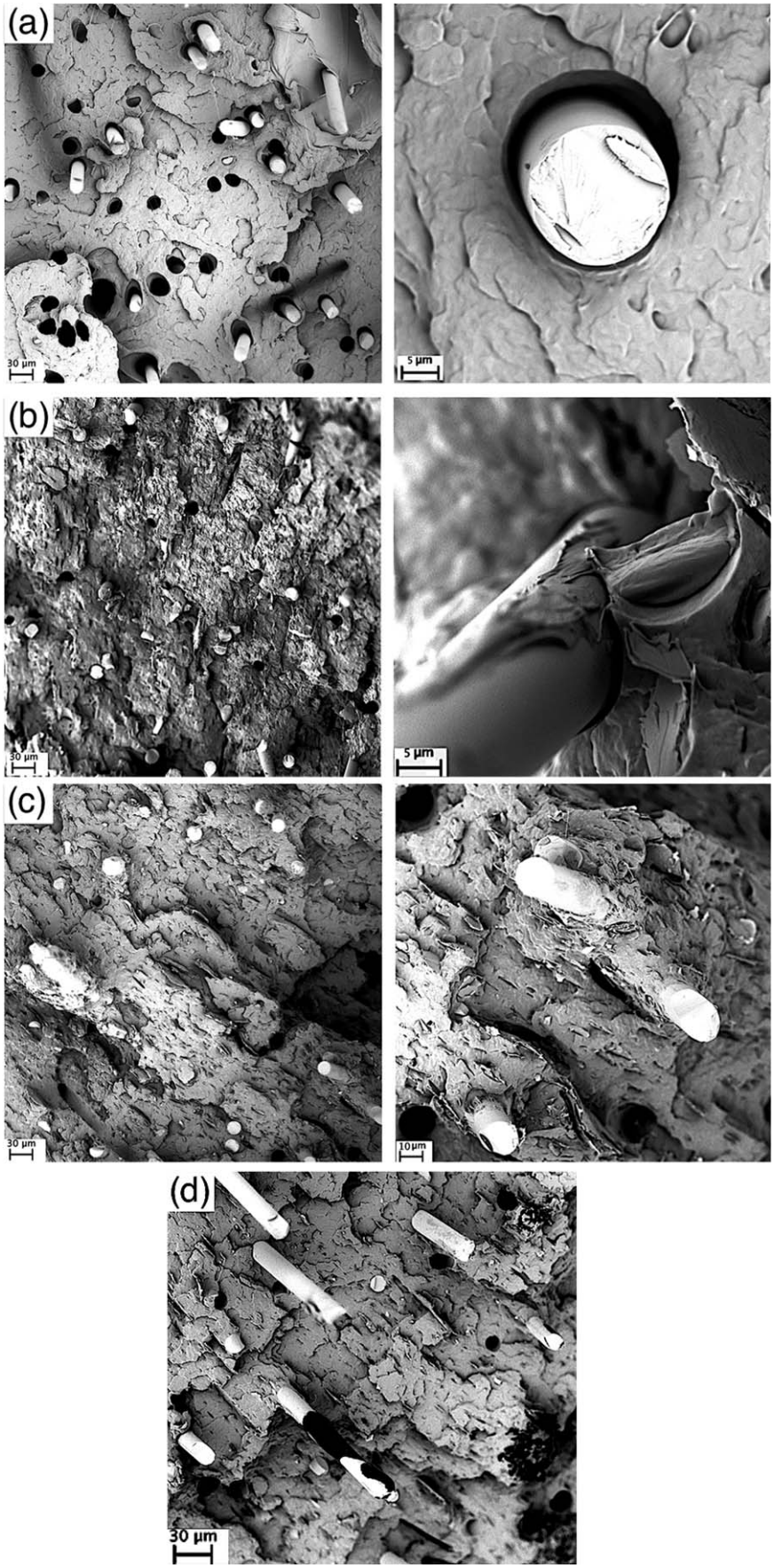

Figure 5. SEM micrographs of fracture surfaces of (a) 10GF/PP, (b) 5GNP/10GF/PP, (c) 5GNP/10GF/5PP-g-MA/PP, and (d) 5GNP/10GFc/PP composites.

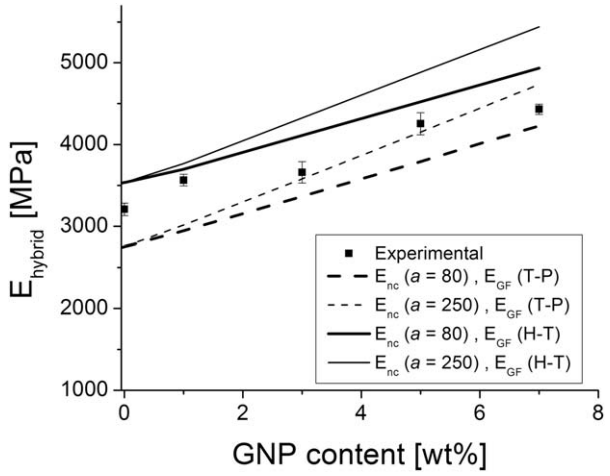

Figure 6. Comparison of elastic modulus predictions with respect to experimental values of GNP/10GF/PP composites for different GNP contents. Predictions based on the additive two-population model applying the Halpin–Tsai theory (E_{nc}, E_{GF} (H-T)) and the Halpin–Tsai and Tsai–Pagano models (E_{nc}, E_{GF} (T-P)) for different GNP aspect ratios.

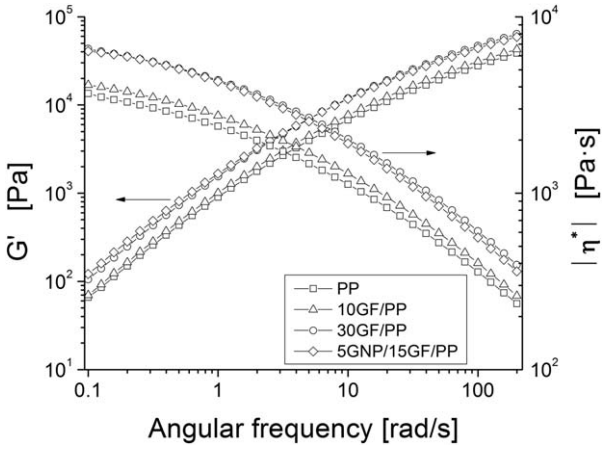

Figure 7. Complex viscosity $|\eta^*|$ and storage modulus (G') with respect to angular frequency (ω) of PP composites.

is reported in Figure 7 as a function of frequency at constant temperature. As expected, both G' and $|\eta^*|$ significantly increase with the GF loading over the tested frequency range and a further increase is observed upon addition of GNP. This effect was also expected, as addition of nanofillers in thermoplastics is associated with an increase of $|\eta^*|$ and G' due to a pseudo solid-like transition caused by the dispersed nanoparticles.[31,32] Interestingly, the sample 5GNP/15GF/PP exhibits values of viscosity comparable with those of 30GF/PP, indicating that for the same content the nanofiller results in a greater increase in viscosity than GF. It is noted that the density of the GNP is significantly lower than that of GF (1.83 ± 0.02 vs. 2.49 ± 0.01 g/cm^3, respectively, as experimentally measured by helium pycnometry) and the nanofiller specific surface area is almost two orders of magnitude greater than that of GF (150 vs. 0.3–2 m^2/g, respectively, based on info by the supplier). Thus it is apparent that the filler surface area is the characteristic that dominates the rheological properties. Moreover, the higher viscosity exhibited by the hybrid composite might also be attributed to the pinning effect of the nanofiller onto the polymeric chains, as evidenced by its higher glass transition temperature (T_g) compared to the non-hybrid composite 30GF/PP (Table II).

The dynamic mechanical properties of the composites were also influenced by the fiber and GNP content: (i) the storage modulus (E') increases with GF (Table II), while the loss tangent decreases, (ii) E' substantially increases with GNP in 10 GF/PP composites, and (iii) the glass transition temperature (T_g), determined as the temperature of the tanδ peak, increases also with GNP. As changes in T_g are related to the primary relaxation of polymer chains and the extent of the immobilized chains, the alteration of polymer chain mobility promoted by polymer–GNP physical interactions might significantly contribute to the reinforcing mechanisms. Therefore in case of GNP, in addition to the stiffening effect, there is a secondary reinforcing mechanism of PP through the significant changes GNP causes on the physical properties of the polymer. In the same way, lower values of tan δ recorded upon GNP addition in hybrid composites can be attributed not only to a stiffening effect and

Table II. Thermomechanical Properties of the Composites

Sample	E' (−20°C) (GPa)	E' (+23°C) (GPa)	T_g (°C)	tan$\delta_{Tg} \times 10^{-2}$
PP	2.97 ± 0.01	1.48 ± 0.01	15.1 ± 0.1	7.89 ± 0.11
10GF/PP	4.62 ± 0.03	2.95 ± 0.01	16.0 ± 0.1	6.15 ± 0.72
30GF/PP	5.99 ± 0.03	4.24 ± 0.02	16.1 ± 0.1	5.21 ± 0.91
1GNP/10GF/PP	4.67 ± 0.03	3.11 ± 0.04	16.2 ± 0.2	6.03 ± 0.73
3GNP/10GF/PP	4.98 ± 0.04	3.24 ± 0.04	16.2 ± 0.1	5.94 ± 0.71
5GNP/10GF/PP	5.13 ± 0.04	3.40 ± 0.03	16.9 ± 0.2	5.88 ± 0.90
7GNP/10GF/PP	5.46 ± 0.04	3.72 ± 0.03	16.9 ± 0.1	5.75 ± 0.62
5GNP/15GF/PP	5.67 ± 0.04	3.85 ± 0.03	17.0 ± 0.1	5.41 ± 0.43
5GNP/10GF/5PPgMA/PP	5.23 ± 0.03	3.43 ± 0.02	17.4 ± 0.1	5.73 ± 0.54

E' (−20°C): Storage modulus at −20°C.
E' (+23°C): Storage modulus at +23°C.
T_g: Glass transition temperature as evaluated in tan δ plot.
tanδ_{Tg}: value of tan δ peak.

the enhanced fiber–matrix adhesion, but also to polymer–GNP physical interactions, resulting in lower loss modulus and enhanced elastic modulus of PP.

CONCLUSIONS

In this study, the mechanical and viscoelastic properties of hybrid PP composites containing GNP and short GFs are determined as a function of the GNP content. The investigation of the fiber–matrix interfacial adhesion and the morphological observations indicated a remarkable increase of the interfacial interactions between matrix and GFs due to the dispersion of GNP in the polymer matrix.

The stronger adhesion combined with the enhancement of the matrix properties result in superior tensile properties and impact resistance and improved viscoelastic behavior. A two-population model, based on the H-T and T-P composite theories, was used to predict the elastic modulus of the hybrid composites. Comparison with the experimental results indicates that the model can satisfactory provide the upper and lower limits of the modulus of the hybrid composites, limits that depend on the aspect ratio (agglomeration) of the nanomaterial and the orientation of the both GNP and GF. Finally, it is concluded that these hybrid composites can be a light-weight alternative to short GF-reinforced thermoplastics.

REFERENCES

1. Piggot, M. R. Load Bearing Fibre Composites; Pergamon Press: Oxford, **1980**.
2. Chamis, C. C. *J. Reinf. Plast. Compos.* **2007**, *26*, 987.
3. Evans, A. G.; Zok, F. W. *J. Mater. Sci.* **1994**, *29*, 3857.
4. Jacob, S.; Suma, K. K.; Mendez, J. M.; George, K. E. *Mater. Sci. Eng. B.* **2010**, *168*, 245.
5. Karger-Kocsis, J., Ed. Polypropylene: An A-Z Reference; Kluwer Publishers: Dordrecht, The Netherlands, **1999**.
6. Pegoretti, A.; Ricco, T. *Compos. Sci. Technol.* **1999**, *59*, 1055.
7. Pedrazzoli, D.; Dorigato, A.; Pegoretti, A. *J. Nanosci. Nanotechnol.* **2012**, *12*, 4093.
8. Tait, M.; Pegoretti, A.; Dorigato, A.; Kalaitzidou, K. *Carbon.* **2011**, *49*, 4280.
9. Hussain, F. *J. Compos. Mater.* **2006**, *40*, 1511.
10. Du, M.; Guo, B.; Jia, D. *Eur. Polym. J.* **2006**, *42*, 1362.
11. Dorigato, A.; Pegoretti, A.; Frache, A. *J. Therm. Anal. Calorim.* **2012**, *109*, 863.
12. Gibson, R. F. *Compos. Struct.* **2010**, *92*, 2793.
13. Kalaitzidou, K.; Fukushima, H.; Drzal, L. T. *Carbon.* **2007**, *45*, 1446.
14. Etcheverry, M.; Ferreira, M. L.; Capiati, N. J.; Pegoretti, A.; Barbosa, S. E. *Compos. Part A* **2008**, *39*, 1915.
15. Pedrazzoli, D.; Pegoretti, A. *Compos. Part A* **2014**, *66*, 25.
16. Ganguli, S.; Roy, A. K.; Anderson, D. P. *Carbon* **2008**, *46*, 806.
17. Wu, H.; Drzal, L. T. *Polym. Compos.* **2013**, *34*, 2148.
18. Isitman, N. A.; Gunduz, H. O.; Kaynak, C. *Polym. Degrad Stab.* **2009**, *94*, 2241.
19. Vlasveld, D. P. N.; Parlevliet, P. P.; Bersee, H. E. N.; Picken, S. J. *Compos. Part A* **2005**, *36*, 1.
20. Herrerafranco, P. J.; Drzal, L. T. *Composites* **1992**, *23*, 2.
21. Fu, S.-Y.; Lauke, B. *Compos. Sci. Technol.* **1998**, *58*, 389.
22. Halpin, J. C.; Kardos, J. L. *Polym. Eng. Sci.* **1976**, *16*, 344.
23. Spencer, M. W.; Cui, L.; Yoo, Y.; Paul, D. R. *Polymer* **2010**, *51*, 1056.
24. Yoo, Y.; Spencer, M. W.; Paul, D. R. *Polymer* **2011**, *52*, 180.
25. Karevan, M.; Pucha, R. V.; Bhuiyan, M. A.; Kalaitzidou, K. *Carbon Lett.* **2011**, *11*, 325.
26. Mallick, P. K. Fiber-Reinforced Composites: Materials, Manufacturing, and Design; Marcel Dekker, Inc.: New York, **1993**.
27. Tsai, S. W.; Pagano, Progress in materials science series, Halftone, J. C., and Pagano, N. J. Eds., Technomic, Stamford (CT), **1968**, 233.
28. Pedrazzoli, D.; Pegoretti, A. *Compos. Sci. Technol.* **2013**, *76*, 77.
29. Kalaitzidou, K.; Fukushima, H.; Drzal, L. T. *Compos. Part A* **2007**, *38*, 1675.
30. Pedrazzoli, D.; Pegoretti, A.; Kalaitzidou, K. *Polym. Eng. & Sc.* **2014**, in press, DOI: 10.1002/pen.23941.
31. Abdel-Goad, M.; Pötschke, P. *J. Non Newtonian Fluid Mech.* **2005**, *128*, 2.
32. Sarvestani, A. S. *Eur. Polym. J.* **2008**, *44*, 263.